PHYSICAL REVIEW B **83**, 241309(R) (2011)

Ternary tetradymite compounds as topological insulators

Lin-Lin Wang[1,*] and Duane D. Johnson[1,2,†]
[1]*Division of Materials Science and Engineering, Ames Laboratory, Ames, Iowa 50011, USA*
[2]*Department of Materials Science and Engineering, Iowa State University, Ames, Iowa 50011, USA*

(Received 20 December 2010; revised manuscript received 18 May 2011; published 29 June 2011)

Ternary tetradymites Bi_2Te_2S, Bi_2Te_2Se, and Bi_2Se_2Te are found to be stable, bulk topological insulators via theory, showing band inversion between group V and VI p_z orbitals. We identify Bi_2Se_2Te as a good candidate to study massive Dirac fermions, with a (111) cleavage-surface-derived Dirac point (DP) isolated in the bulk-band gap at the Fermi energy (E_f)-like Bi_2Se_3 but with a spin texture alterable by layer chemistry. In contrast, Bi_2Te_2S and Bi_2Te_2Se (111) behave like Bi_2Te_3, with a DP below E_f buried in bulk bands. Bi_2Te_2S offers large bulk resistivity needed for devices.

DOI: 10.1103/PhysRevB.83.241309 PACS number(s): 73.43.−f, 72.25.Hg, 73.20.−r, 85.75.−d

Materials that exhibit topological insulator (TI) behavior reveal a novel quantum state for electrons,[1,2] where surface states of a three-dimensional (3D) system are topologically protected against disorder by time-reversal symmetry (TRS) and, as a result, electrons experiences no backward scattering by nonmagnetic impurities. The unique feature of a 3D TI lies in its band dispersion—surface bands connect valence and conduction bands and cross the Fermi level E_f an odd number of times along two TRS-equivalent k points, typically found in narrow-gap semiconductors with strong spin-orbit coupling (SOC). Since Bi_2Se_3 and Bi_2Te_3 were concurrently observed[3–5] and predicted[6] to be 3D TI, an intensive search[7–10] continues for other systems. Notably, Bi_2Se_3 and Bi_2Te_3 belong to a class of line compounds called *tetradymites*. Ternary tetradymites, such as Bi_2Te_2S, Bi_2Te_2Se, and Bi_2Se_2Te are also stable[11,12] and potentially offer a "chemistry knob" to control TI behavior. Here, we provide insight for device development—cleavage surface-band dispersion and location of Dirac point (DP) both relative to bulk bands, as well as the warping (out-of-plane spin component, referred hereafter as *spin texture*) of the Dirac cone (DC).

Upon band inversion and crossing of E_f due to SOC, a DP is formed leading to variety of unique physics. Using angle-resolved photoelectron spectroscopy, Chen *et al.*[13] have shown that massive Dirac fermion is produced on Bi_2Se_3 (111) surface by breaking TRS via magnetic impurities. To do this, the position of DP must be in the gaps of both bulk and surface bands. Bi_2Se_3 has a DP isolated in the bulk-band gap region making it a good candidate for such studies, whereas the DP for Bi_2Te_3 is below E_f and buried among surface-valence bands (Fig. 4 in Ref. 6). Also, Bi_2Se_3 has a larger band gap compared to Bi_2Te_3, offering more control at elevated temperature. Another large difference between the binary tetradymites is the shape of DC. In contrast to the perfect DC of Bi_2Se_3, Bi_2Te_3 exhibits warping and a spin texture,[14,15] suggested to form exotic charge and spin-density waves. Importantly, then, it is more helpful for theory to predict not only TI but also to detail surface-band dispersion.

Although the calculated[7] bulk bands of Bi_2Te_2Se and Bi_2Te_2S indicate TI behavior, with Bi_2Te_2Se confirmed experimentally,[16] the positions of surface-derived DP and DC features (spin texture) have not been analyzed. Also, there has been no study on Bi_2Se_2Te. We focus on bulk and surface band TI features of these ternary tetradymites as calculated in density functional theory[17,18] (DFT). We analyze both the bulk and surface (via a slab model) band structures to identify any 3D TIs along with the nature of the DP, especially its location and shape of DC. We find that all of them are 3D TIs, with Bi_2Te_2S and Bi_2Te_2Se behaving like Bi_2Te_3, but with higher impurity formation energy than Bi_2Te_3, suggesting lower bulk conductivity. We also present band dispersion for two TI Bi_2Se_2Te structures (a variant of a partially disordered structure, verified as the lowest-energy structure, and a hypothetical structure) to address the effect of site substitution (chemistry) on the DC and spin texture.

One costly method to tell a TI from an ordinary band insulator is to calculate the Z_2 topological order parameter.[19] Yet, for structures with inversion symmetry, Fu *et al.*[20] proposed inspecting the parity product of occupied bands on TRS equivalent k points in the bulk bands. Here, we search for a band inversion and zero gap in bulk bands by tuning the SOC (λ from 0 to 100%), and then, once verified, we calculate surface bands and assess DP formation, an approach used for semi-infinite surfaces of the binaries by Zhang *et al.*[6]

Tetradymite compounds formed between group V and VI elements have a quintuple-layered structure, in which group VI element occupies the outmost and central (third) layer, and group V element occupies the second layer, e.g., for Bi_2Se_3, the layers stack as Se^{I}-Bi-Se^{II}-Bi-Se^{I} along ⟨111⟩ in the primitive rhombohedral cell with the space group of $R\bar{3}m$ (No. 166). The two group VI positions are not equivalent. The stacking is similar to fcc, but the interlayer distances are different; in particular, the distance between neighboring quintuple-layer units is the largest, making it easier to cleave with group VI element exposed as the surface layer. We use DFT with PW91 exchange-correlation functional[21] and plane-wave basis set with projected augmented waves,[22] as implemented in VASP.[23,24] Bulk tetradymite can also be represented as a hexagonal lattice with 15 atomic layers, which also gives the basis in the slab model for the (111) surface. Both the atomic structure and Brillouin zone for tetradymite bulk and (111) surface have been shown before,[6,25] so we do not repeat them. For bulk we use the primitive rhombohedral cell of five atoms with 7×7×7 k-point mesh. We use a three quintuple-layered slab along ⟨111⟩ with no vacuum for bulk band projection and a 14 Å vacuum for surface-band calculations. The kinetic

TABLE I. Experimental (Refs. 11 and 12) structural parameters (a, c and internal parameters x_1 and x_2) and DFT-PW91 results for bulk tetradymite compounds, i.e., critical strength of SOC for band inversion at Γ point (λ_c), lowest band gap along high-symmetry directions (Δ_{hs}) considered and band gap at Γpoint (Δ_Γ).

	a (Å)	c (Å)	x_1	x_2	λ_c	Δ_{hs} (eV)	Δ_Γ(eV)
Bi_2Se_3	4.138	28.64	0.399	0.206	0.46	0.32	0.47
Bi_2Te_3	4.383	30.487	0.400	0.212	0.48	0.14	0.52
Bi_2Se_2Te	4.218	29.240	0.398	0.211	0.71	0.17	0.25
Bi_2Te_2Se	4.28	29.86	0.396	0.211	0.21	0.28	0.70
Bi_2Te_2S	4.316	30.01	0.392	0.212	0.44	0.28	0.53

energy cutoff is 280 eV. The k-point meshes used are 10×10×2 and 10×10×1, respectively. The convergence with respect to k-point mesh was carefully checked, with total energy converged, e.g., well below 1 meV/atom. We use experimental lattice constants (Table I) and fix atoms in their bulk positions. To show a TI surface band connects conduction and valence bands, a semi-infinite surface is required[6] and achieved with a thick-slab model.[26] At least three quintuple layers along ⟨111⟩ are needed to model the band dispersion in semi-infinite surface with the group VI terminated surfaces well separated by 28 Å. We provide validation of our surface-band structure for binary Bi_2Se_3 and Bi_2Te_3 in the supporting materials.[27]

In tetradymites, central-layer substitution is commonly observed, e.g., Bi_2Te_2S and Bi_2Te_2Se.[11,12] For Bi_2Se_2Te, the structure with Te substituting for Se in the central layer of Bi_2Se_3 (we call Bi_2Se_2Te-I) has not been observed. However, we have calculated that a partially disordered structure (we call Bi_2Se_2Te-II) suggested from x-ray diffraction[12] is a very low-energy structure, in which half of the Se in the outer layers are replaced randomly with Te, which conforms to Hume-Rothery solid-solution rules. To assess behavior, we used an ordered (2×2) supercell approximate for the partially disordered structure. Because our focus is on electronic structure and TI behavior, we include both Bi_2Se_2Te-I and Bi_2Se_2Te-II and show the chemistry effects on band dispersion. The details in structural complexity, energetics, and phase diagram of Bi_2Se_3-Bi_2Te_3 will be reported later.[28]

For the prototype ternary tetradymite, Bi_2Te_2S, where Te in the central layer of Bi_2Te_3 is replaced with S, a slightly smaller lattice constant is found, see Table I. The bulk band, Fig. 1(c), shows an indirect gap along high-symmetry directions (Δ_{hs}) of 0.28 eV. We also calculate the band gap at Γ point (Δ_Γ) versusλ (with charge density fixed at that of $\lambda = 0$). As seen in Fig. 1(d), $\Delta_\Gamma$becomes 0 around the critical value $\lambda_c = 44\%$. Compared to the band structure without SOC in Fig. 1(a), the largest change is the lowering of the lowest-conduction band and the rising of the highest-valence band to form jointly a DP at Γ point at E_f. Upon further increase of λ, Fig. 1(c) shows that the gap at Γ point is reopened and two nearby maximum are formed. Figure 1(e) shows the projections of the lowest-conduction band on Bi and Te p_z orbital versus λ. Below (above) 44% SOC, it is mostly composed of Bi (Te) p_z components. Indeed, SOC causes the band inversion in Bi_2Te_2S, similar to the binaries,[6] so Bi_2Te_2S is also a 3D TI. The data in Table I may be useful for device development.

To see the surface bands of $Bi_2Te_2S(111)$, we plot in Fig. 1(f) the dispersion of a three-quintuple slab on top of the projected bulk bands. Similar to Bi_2Te_3 [see Fig. S1(d)], we find the DP for $Bi_2Te_2S(111)$ is below E_f and buried by other states around the Γ point, showing that the two outmost surface layers in tetradymite determine the position of DP.

Ternary Bi_2Te_2Se is similar to Bi_2Te_2S, with the central Te layer in Bi_2Te_3 replaced by Se. In Figs. 2(a) and 2(b) we show its bulk and surface band dispersion. By tuning λ, we find that the bulk band inversion occurs when $\lambda_c = 21\%$ (Table I). Thus, Bi_2Te_2Se is also a 3D TI, with a Δ_{hs} of 0.28 eV—larger than that of Bi_2Te_3, mostly due to a smaller lattice constant. Looking at slab surface bands, we find similar features to that of Bi_2Te_3 for the position of DP; i.e., the DP of Bi_2Te_2Se is buried deeper below E_f (−0.08 eV) than that of Bi_2Te_3 (−0.02 eV) and Bi_2Te_2S (−0.05 eV); see Fig. 2.

Figures 2(c) and 2(d) show bulk and surface dispersions for the hypothetical Bi_2Se_2Te-I, where Te replaces Se in the central layer of Bi_2Se_3. At $\lambda_c = 71\%$, a band inversion at the Γ point for bulk indicates that it is a 3D TI. The surface bands in Fig. 2(d) show that it behaves much like Bi_2Se_3 with the DP located in the gap region and not buried by other valence bands. In contrast, if Te substitutes instead in the outer layers, consistent with Hume-Rothery's rules, we find the Bi_2Se_2Te-II surface band structure in Fig. 2(e), where the highest-valance band around Γ point becomes more flat (beyond the effect of

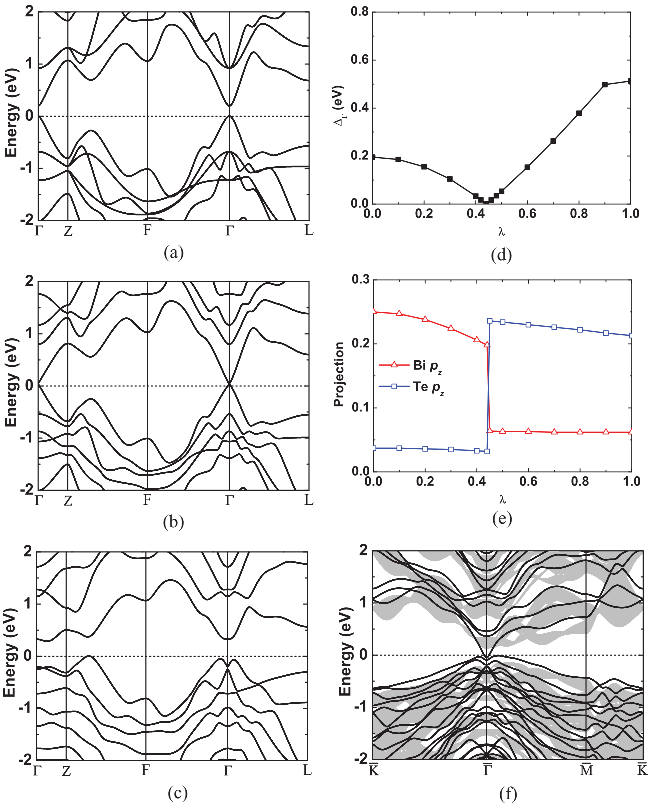

FIG. 1. (Color online) Band structures of bulk Bi_2Te_2S are shown with SOC strength (λ) of 0, 44, and 100% in (a), (b), and (c), respectively. (d) Bulk-band gap at Γ point vs. λ. (e) Projection of the lowest conduction band at Γ point on Bi and Te p_z orbital vs. λ. (f) Band structure of a Bi_2Te_2S slab.

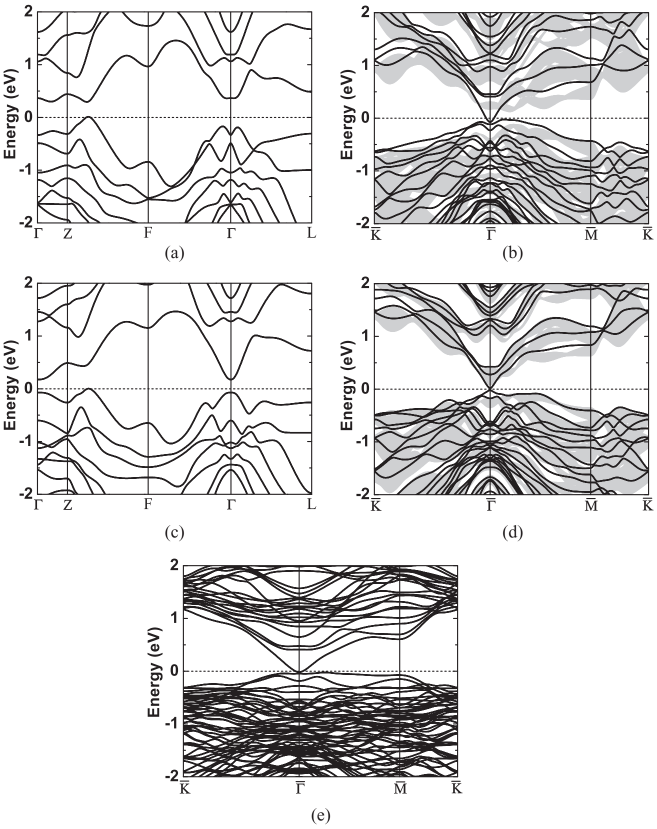

FIG. 2. Band structure with full SOC for Bi_2Te_2Se and Bi_2Se_2Te. For Bi_2Te_2Se, we show (a) bulk dispersion and (b) slab dispersion along ⟨111⟩. For Bi_2Se_2Te-I, (c) and (d) are similar to (a) and (b). For Bi_2Se_2Te-II, we show slab dispersion (e) along ⟨111⟩ (no bulk for clarity).

zone folding), and the isolation of the DP in the gap region remains but is less prominent than for Bi_2Se_2Te-I. This direct comparison again shows that the outer two surface layers mostly determined the locations of the valence band and DP.

A significant difference between the surface band structures of Bi_2Se_3 and Bi_2Te_3 is the shape of DC and the associated spin texture. Figure 3 shows the shape of the conduction band of each compound around the Γ point. Comparing Figs. 3(a) and 3(d), the DC for Bi_2Te_3 remains ideal up to 0.2 eV above E_f, while for Bi_2Se_3 it is 0.4 eV, agreeing with previous experiments[5,13] and theory.[14,15] Above these energies, there is significant warping of the DC for Bi_2Te_3, as evidenced by the change in the shape—first to a hexagon, then to a snowflake. Such nonconvex shapes produce more pairs of stationary points on the constant-energy contours, allowing scattering processes among different pairs of stationary points. This result is in contrast to no scattering for a convex DC as observed in STM experiment,[29] where a line defect on $Bi_2Te_3(111)$ suppresses scattering only in the energy range of circular constant-energy contours, not snowflake types.

Figure 3 also shows the spin texture associated with the DC, i.e., the ratio of out-of-plane to total electron-spin moment color-mapped on the cone. For a perfect DC, the electron spin always lies in the surface plane and is perpendicular to the wave vector. In contrast, for a warped DC, Fu[14] suggested that there should be a significant amount of out-of-plane spin moments (up to 60%) to maintain a Berry phase change of π in one circuit, as required by topological invariance. Such behavior can lead to interesting features, such as spin-density waves on a 3D TI surface and opening of DP by an in-plane magnetic field. For Bi_2Te_3, our results in Fig. 3(a) agree with a previous calculation[15] and show a large spin texture above 0.2 eV, except for $\overline{\Gamma}-\overline{M}$. In contrast, Bi_2Se_3 has a much smaller spin texture [Fig. 3(d)]. For Te-rich ternaries, compared to Bi_2Te_3, the upper warping limit of the cone convexity for Bi_2Te_2S and Bi_2Te_2Se are both increased to 0.3 eV [see Figs. 3(b) and 3(c)], and beyond that only small spin textures appear, with Bi_2Te_2Se being larger than Bi_2Te_2S. On the Se-rich side, compared to Bi_2Se_3, the upper warping limit of the cone convexity for Bi_2Se_2Te-II [see Fig. 3(e)] is slightly decreased, and beyond that a slightly larger spin texture appears; in contrast, for Bi_2Se_2Te-I [see Fig. 3(f)], the upper warping limit is reduced to 0.3 eV, and a much larger spin texture appears, similar to Bi_2Te_3. Thus, even though the position of DP and dispersion of valence bands are only slightly affected by the substitution of

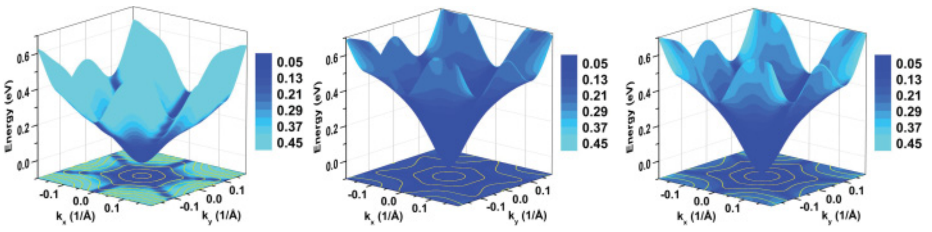

(a) Bi_2Te_3 (b) Bi_2Te_2S (c) Bi_2Te_2Se

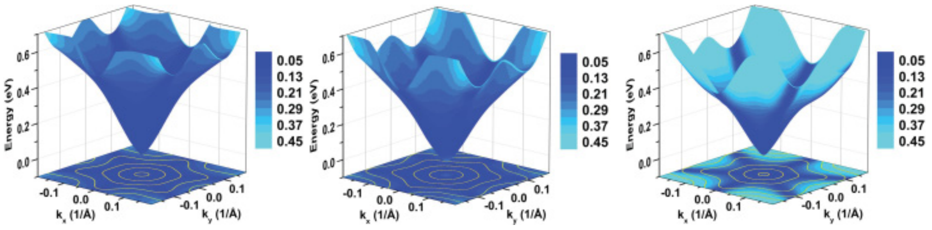

(d) Bi_2Se_3 (e) Bi_2Se_2Te-II (f) Bi_2Se_2Te-I

FIG. 3. (Color online) Spin texture color-mapped on the conduction-band Dirac cone for the binary and ternary compounds studied (the hypothetical Bi_2Se_2Te-I shows the chemistry effect). Color indicates the amount of out-of-plane electronic spin moment in percentage. Constant-energy contours are drawn on bottom.

Te in the central layer (Fig. 2), the warping and spin texture in conduction band are greatly affected by chemical substitutions. The change in the warping limit reflects the stronger trigonal crystal potential of Te than Se and S.

In Bi_2Te_2Se and Bi_2Se_2S, the binding of the site in the central layer to two Bi sites increases hybridization and decreases spin-orbit coupling. While in Bi_2Se_2Te-I, by replacing the central Se layer with Te, the spin-orbit coupling in the Bi-Te-Bi trilayer is enhanced and results in a large spin texture. Thus, introducing Te into the central layer of Bi_2Se_3 can make a superb TI candidate with a DP standing alone in bulk band gap (just like Bi_2Se_3) as well as a large spin texture (just like Bi_2Te_3 and larger than Bi_2Se_3). But finding feasible ways to introduce Te into the central layer poses a challenge. However, while spin texture in Bi_2Se_2Te-II is not as large as that in Bi_2Se_2Te-I, it is larger than Bi_2Se_3. All other electronic features are similar, including isolation of the DP in the gap, suggesting the lower-energy, partially disordered structure will also be a superb TI candidate.

Last, any potential use of these materials as a 3D-TI device requires control over the bulk resistivity. Binary tetradymites Bi_2Se_3 and Bi_2Te_3 are semiconductors, but defects (such as vacancy and Bi-Te-antisite) cause significant bulk conductivity, which overwhelms the surface-state contribution. For example, Ren *et al.*[16] measured that Bi_2Te_2Se has a much larger bulk resistivity than Bi_2Te_3 because the substitution of the central Te site with Se reduces the formation of a Se vacancy and Bi-Te antisite. The same mechanism should also be operative for Bi_2Te_2S because S is more electronegative and binds Bi stronger than Se, preserving the stoichiometric structure even better than Bi_2Te_2Se. For example, the energy cost to create a Bi-Te-antisite pair is increased by 0.06 eV when changing from Bi_2Te_2Se to Bi_2Te_2S.[28] A similar situation holds for quaternary $Bi_2(Te\text{-}Se)_2S$.

In conclusion, we find that Bi_2Te_2S, Bi_2Te_2Se and Bi_2Se_2Te ternary tetradymites are bulk topological insulators, confirmed computationally by verifying band inversion between group V and VI p_z orbitals. We validated and then used band structures of a large (three quintuple-layered) slab model to study surface-band features, including the warping of DC and its associated spin texture. The location of the DP for Bi_2Te_2Se and Bi_2Te_2S (111) surfaces is like that of Bi_2Te_3. We also present dispersion for the energetically preferred *partially disordered* Bi_2Se_2Te (via an ordered approximate) that showed it had a favorably located surface-derived DP near E_f in the bulk-band gap like Bi_2Se_3 but with a larger spin texture. We studied a hypothetical Bi_2Se_2Te structure to show that substitution in the central layer affects the shape of DC and the associated spin texture, while substitution in outer layers affects the location of the DP and dispersion of valence band. Due to high defect-formation energy, Bi_2Te_2S should have a large bulk resistivity needed to realize a workable device.

Work at Ames Laboratory was supported by the US Department of Energy, Office of Basic Energy Sciences, Division of Materials Science and Engineering. Ames Laboratory is operated for DoE by Iowa State University under Contract No. DE-AC02-07CH11358.

---

[*] llw@ameslab.gov
[†] ddj@ameslab.gov

[1] X. L. Qi and S. C. Zhang, Phys. Today **63**(1), 33 (2010).
[2] M. Z. Hasan and C. L. Kane, Rev. Mod. Phys. **82**, 3045 (2010).
[3] Y. Xia *et al.*, Nat. Phys. **5**, 398 (2009).
[4] D. Hsieh *et al.*, Phys. Rev. Lett. **103**, 146401 (2009).
[5] Y. L. Chen *et al.*, Science **325**, 178 (2009).
[6] H. J. Zhang, C. X. Liu, X. L. Qi, X. Dai, Z. Fang, and S. C. Zhang, Nat. Phys. **5**, 438 (2009).
[7] M. Klintenberg, e-print arXiv:1007.4838v1 (2010).
[8] S.-Y. Xu *et al.*, e-print arXiv:1007.5111v1 (2010).
[9] B. Yan, H.-J. Zhang, C.-X. Liu, X.-L. Qi, T. Frauenheim, and S.-C. Zhang, Phys. Rev. B **82**, 161108(R) (2010).
[10] H. Jin, J.-H. Song, A. J. Freeman, and Kanatzidis M. G., Phys. Rev. B **83**, 041202(R) (2011).
[11] R. W. G. Wyckoff, *Crystal Structures*, 2nd ed. (Wiley-Interscience, New York, 1965).
[12] S. Nakajima, J. Phys. Chem. Solids **24**, 479 (1963).
[13] Y. L. Chen *et al.*, Science **329**, 659 (2010).
[14] L. Fu, Phys. Rev. Lett. **103**, 266801 (2009).
[15] M. Z. Hasan, H. Lin, and A. Bansil, Physics **2**, 108 (2009).
[16] Z. Ren, A. A. Taskin, S. Sasaki, K. Segawa, and Y. Ando, Phys. Rev. B **82**, 241306(R) (2010).
[17] P. Hohenberg and W. Kohn, Phys. Rev. B **136**, B864 (1964).
[18] W. Kohn and L. J. Sham, Phys. Rev. **140**, 1133 (1965).
[19] C. L. Kane and E. J. Mele, Phys. Rev. Lett. **95**, 146802 (2005).
[20] L. Fu and C. L. Kane, Phys. Rev. B **76**, 045302 (2007).
[21] J. P. Perdew and Y. Wang, Phys. Rev. B **45**, 13244 (1992).
[22] P. E. Blöchl, Phys. Rev. B **50**, 17953 (1994).
[23] G. Kresse and J. Furthmuller, Phys. Rev. B **54**, 11169 (1996).
[24] G. Kresse and J. Furthmuller, Comput. Mater. Sci. **6**, 15 (1996).
[25] W. Zhang, R. Yu, H. J. Zhang, X. Dai, and Z. Fang, New J. Phys. **12**, 065013 (2010).
[26] Oleg V. Yazyev, Joel E. Moore, and Steven G. Louie, Phys. Rev. Lett. **105**, 266806 (2010).
[27] See Supplemental Material at http://link.aps.org/supplemental/10.1103/PhysRevB.83.241309 for band structures of Bi_2Se_3 and Bi_2Te_3.
[28] L.-L. Wang, A. Alam, D. D. Johnson, M. Huang, S. Thimmaiah, and T. A. Lograsso (in preparation, 2011).
[29] Z. Alpichshev, J. G. Analytis, J. H. Chu, I. R. Fisher, Y. L. Chen, Z. X. Shen, A. Fang, and A. Kapitulnik, Phys. Rev. Lett. **104**, 016401 (2010).